Criticality in the quantum kicked rotor with a smooth potential

Rina Dutta and Pragya Shukla
Department of Physics, Indian Institute of Technology, Kharagpur, India
(Received 14 May 2008; published 10 September 2008)

We investigate the possibility of an Anderson-type transition in the quantum kicked rotor with a smooth potential due to dynamical localization of the wave functions. Our results show the typical characteristics of a critical behavior, i.e., multifractal eigenfunctions and a scale-invariant level statistics at a critical kicking strength which classically corresponds to a mixed regime. This indicates the existence of a localization to delocalization transition in the quantum kicked rotor. Our study also reveals the possibility of other types of transition in the quantum kicked rotor, with a kicking strength well within the strongly chaotic regime. These transitions, driven by the breaking of exact symmetries, e.g., time reversal and parity, are similar to weak-localization transitions in disordered metals.

DOI: 10.1103/PhysRevE.78.031115 PACS number(s): 05.40.−a, 05.45.−a, 05.90.+m, 05.70.Fh

I. INTRODUCTION

The analogy of the statistical fluctuations of dynamical systems and disordered systems is well known in the delocalized wave regime (corresponding to the metallic limit in disordered systems and the classically chaotic limit in dynamical systems) and has been explained using random matrix theory as a tool [1–4]. A similar analogy exists for fully localized regimes of the wave functions too (i.e., between the insulator limit of disordered systems and the integrable limit of dynamical systems) [1–3]. It is therefore natural to probe the presence or absence of the analogy in partially localized or critical regimes of these systems. Our analysis shows that, similar to the $d>2$ Anderson Hamiltonian (d as dimension), the $d=1$ quantum kicked rotor (QKR) undergoes a localization-delocalization transition in the classically mixed regime. We also find quantum phase transitions in its chaotic regime due to breaking of the symmetries, e.g., time reversal and parity, in the quantum system. As in disordered systems, the symmetry-breaking transitions in the QKR occur due to weak-localization effects. Similar phase transitions due to symmetry breakings have been seen in a few other complex systems too, e.g., ensembles of distinguishable spins [5].

The connection of the kicked rotor to the $d=1$ Anderson Hamiltonian has been known for several decades [2,6–8]. A recent work [9] further explores the connection and shows that, for the nonanalytic potentials in the QKR, the eigenstates show multifractality or power-law localization [10–13], a behavior similar to the eigenstates of a $(d>2)$-dimensional Anderson Hamiltonian [14] at its critical point. Our study shows the existence of multifractal eigenstates in the QKR with smooth potentials too, e.g., $V(q)=K\cos(q)$ in specific parametric conditions. Furthermore, as in a critical Anderson system, the multifractality in the QKR is accompanied by a critical level statistics (size independent and different from that at the two ends of the transition), a necessary criterion for critical behavior [10]. This indicates a much deeper connectivity of the kicked rotor to the Anderson Hamiltonian, not affected just by the nature of the potential or the dimension of the system. As discussed here, the connection seems to be mainly governed by the "degree of complexity" (measured by a complexity parameter discussed later) and may exist among a wider range of dynamical and disordered systems.

The present study is motivated by a recent analytical work [15,16] leading to a common mathematical formulation for the statistical fluctuations of a wide range of complex systems. The work, based on ensemble averaging, shows that the fluctuations are governed by a single parameter Λ in addition to global constraints on the system [15,16]. Λ, referred to as the complexity parameter, turns out to be a function of the average accuracy of the matrix elements, measured in units of the mean level spacing. The fluctuations in two different systems subjected to similar global constraints are analogous if their complexity parameters are equal, irrespective of other system details.

The Λ formulation was recently used by us to find the Gaussian Brownian ensemble (GBE) [17] and the power-law random banded matrix ensemble (PRBME) [18] analogs of the Anderson ensemble (AE) (for arbitrary d) [19]. However, it cannot directly be applied to find the QKR analog; this is, in principle, due to the inapplicability of ensemble averaging to dynamical systems. Fortunately it is possible to derive Λ for dynamical systems by a semiclassical route, using phase-space averages [20]. The semiclassical Λ was used by us [20,21] to map the statistics of the time-evolution operator U of the QKR to that of the circular Brownian ensemble (CBE) [17]. The lack of a suitable criterion for the critical statistical behavior prevented us earlier from a critical QKR analysis. Our present work pursues the analysis by first analytically identifying the critical QKR behavior using the semiclassical $\Lambda\equiv\Lambda_{\mathrm{KR}}$; the limit $N\to\infty$, $\Lambda\to\Lambda^*$ with Λ^* independent of the size N, gives the critical points of transition. This is followed by a numerical analysis of an ensemble of QKRs which confirms critical behavior at the semiclassically predicted values. This in turn suggests a paradoxical validity of the ensemble averaging in dynamical systems at least of QKR type (also indicated by the CBE-QKR mapping). A subsequent comparison of the semiclassical Λ_{KR} to the ensemble-based Λ_{AE} of the Anderson Hamiltonian (arbitrary d) gives us its QKR analog; the analogy is numerically confirmed too.

The statistical behavior in the bulk of the spectrum of a standard Gaussian ensemble is known to be analogous to a standard circular ensemble (for large matrix sizes) [17,22].

Our work extends this analogy to their Brownian ensemble counterparts too, that is, the analogy between the GBE and the CBE (by the mapping GBE→AE→QKR→CBE). This in turn indicates a connection among a wide range of physical systems which are known to be well modeled by the Anderson Hamiltonian, the kicked rotor, and Brownian ensembles of Gaussian and circular type.

The paper is organized as follows. Section II briefly reviews the basic features of the kicked rotor and the Anderson Hamiltonian required for our analysis; it also discusses the parametric conditions in the kicked rotor which can support critical points. Section III deals with the numerical confirmation of the critical level statistics and the multifractality of the eigenfunctions at critical parametric conditions in the QKR and their comparison with a $(d=3)$-dimensional Anderson Hamiltonian. We conclude in Sec. IV with a brief discussion of our main results and open questions.

II. KICKED ROTOR AND ANDERSON HAMILTONIAN

The kicked rotor and the Anderson Hamiltonian have been subjects of intense study in the past and many of their details can be found in several references [1,2,4,8,23]. However, for self-consistency of the paper, we present here a few details required for later discussion.

A. Kicked rotor and complexity parameter

The kicked rotor can be described as a pendulum subjected to periodic kicks (of time period T) with Hamiltonian H given as

$$H = \frac{(p+\gamma)^2}{2} + K\cos(\theta+\theta_0)\sum_{n=-\infty}^{\infty}\delta(t-nT). \tag{1}$$

Here K is the stochasticity parameter, and γ and θ_0 are the time-reversal and parity symmetry breaking parameters in the quantum Hamiltonian when acting in a finite Hilbert space.

Integration of the equations of motion $\dot{\theta}=-\partial H/\partial p$, $\dot{p}=\partial H/\partial\theta$ between subsequent kicks, e.g., n and $n+1$, gives the classical map

$$p_{n+1} = p_n + K\sin(\theta_n+\theta_0) \pmod{2\pi},$$

$$\theta_{n+1} = \theta_n + p_{n+1} \pmod{2\pi}. \tag{2}$$

The map is area preserving and invariant under the discrete translation $\theta\to\theta+2\pi$, $p\to p+2\pi$. It also preserves the time-reversal symmetry $p\to 2\pi-p$, $\theta\to\theta$, $t\to -t$ and the parity symmetry $p\to 2\pi-p$, $\theta\to 2\pi-\theta$ for all values of γ and θ_0. Thus the classical dynamics depends only on K, changing from integrable $(K=0)$ to near integrable $(0<K<4.5)$ to large-scale chaos $(K>4.5)$.

The quantum dynamics can be described by a discrete time-evolution operator $U=G^{1/2}BG^{1/2}$ [2,7] where

$$B = \exp[-ik\cos(\theta+\theta_0)], \tag{3}$$

$$G = \exp[-iT(p+\gamma)^2/2\hbar] = \exp\left[i\tau\left(\frac{\partial}{\partial\theta}-i\frac{\gamma}{\hbar}\right)^2/2\right]. \tag{4}$$

Here $k=K/\hbar$, $\tau=T\hbar$, and θ and $p=i\hbar\partial/\partial\theta$ are the position and momentum operators, respectively; p has discrete eigenvalues, $p|m\rangle=m\hbar|m\rangle$ $(m=1\to N)$ due to periodicity of θ $(\theta\to\theta+2\pi)$. The choice of a rational value for $\tau/4\pi=M/N$ results in a periodicity also for the momentum operator $p'=p+4\pi M/T$ $(l'=l+N)$ and therefore in discrete eigenvalues for θ $[\theta|l\rangle=(2\pi l/N)|n\rangle]$. The quantum dynamics can then be confined to a two-dimensional torus (with a Hilbert space of finite size $N=2\pi m_0/\tau$ with m_0 an integer). The classical analog of this model corresponds to the standard mapping on a torus of size $2\pi m_0/T$ in the momentum p; thus the classical limit is $\tau\to 0$, $k\to\infty$, $N\to\infty$ with $K=$const and $N\tau=$const [2,7].

For the dynamical-localization analysis, it is useful to express the matrix U in the momentum basis [2,2,20]:

$$U_{mn} = \frac{1}{N}\exp[i\tau(m-\gamma/\hbar)^2/4 + i\tau(n-\gamma/\hbar)^2/4] \times\sum_{l=-N_1}^{N_1}\exp[-ik\cos(2\pi l/N+\theta_0)] \times\exp[-2\pi i l(m-n)/N], \tag{5}$$

where $n,m=-N_1,\ldots,N_1$ with $N_1=(N-1)/2$ if N is odd and $N_1=N/2$ if N is even. It is clear that the properties of H, Eq. (1), are recovered in the infinite matrix size limit.

The quantum dynamics under exact symmetry conditions $(\gamma=0,\ \theta_0=0)$ can significantly be affected by relative values of k,τ,N. It was first conjectured [2] and later on verified [20] that the statistical properties are governed by the ratio of the localization length ζ to the total number of states N or, equivalently, k^2/N (as $\zeta=D/2\tau^2$ with $D\approx K^2/2$ as the diffusion constant). However, to the best of our knowledge, the critical behavior at $k^2\simeq N$ was not probed before. The other parameters playing a crucial role in the quantum dynamics are γ and θ_0, the measures of time-reversal and parity symmetry breaking, respectively (with $0<\gamma<\hbar$ and $-\pi/N<\theta_0<\pi/N$). Note that the change of $p\to p+\gamma$ or $\theta\to\theta+\theta_0$ is a canonical transformation, thus leaving the classical Hamiltonian unaffected. The corresponding quantum dynamics, however, is affected as the quantum Hamiltonian acting in a finite Hilbert space may not remain invariant under a unitary transformation.

Following Eq. (5), the multiparametric nature of U is expected to manifest itself in the statistical behavior of its eigenvalues (quasienergies) and the eigenfunctions. However, as shown in [20] using semiclassical techniques, the quasienergy statistics of U is sensitive to a single parameter Λ_{KR} and the exact symmetry conditions. Under exact time-reversal symmetry $(\gamma=0)$ and partially violated parity symmetry $(\theta_0\neq 0)$ (taking $T=1$, equivalently, $\tau=\hbar$, without loss of generality), we have [20]

$$\Lambda_{\mathrm{KR,T}} = \frac{\theta_0^2 N k^2}{4\pi^2} = \frac{N^3 \theta_0^2 K^2}{64\pi^4 M^2}. \tag{6}$$

Note that, for $\theta_0 = \pi/2N$, $\Lambda_{\mathrm{KR,T}}$ is essentially the same as the one conjectured in [2] for scaling behavior of the spectral statistics. Similarly, for the strongly chaotic case ($k^2 > N$) with only parity symmetry ($\theta_0 = \pi/2N$) and no time-reversal symmetry ($\gamma \neq 0$),

$$\Lambda_{\mathrm{KR,NT}} = \frac{\gamma_q^2 N^3}{48\pi^2} \tag{7}$$

with $\gamma_q = \gamma/\hbar$. As Eq. (6) indicates, $\Lambda_{\mathrm{KR,T}} \to \infty$ in the strongly chaotic limit $k \to \infty$; similarly, from Eq. (7), $\Lambda_{\mathrm{KR,T}} \to \infty$ for $\gamma \simeq \hbar$; the statistics in these cases can be well modeled [20,24] by the standard random matrix ensembles of unitary matrices, known as the standard circular ensembles, e.g., the circular orthogonal ensemble (COE), circular unitary ensemble (CUE), etc. [17]. The cases with a slow variation of k, γ, or θ_0 (partial localization, partial time-reversal violation or partial parity violation respectively) and finite size N correspond to a smooth variation of $\Lambda_{\mathrm{KR,T}}$ or $\Lambda_{\mathrm{KR,NT}}$ between 0 and ∞. The intermediate statistics for these cases [20,21] can be well described by the circular Brownian ensembles. The latter are ensembles of unitary matrices, described as $U_w = U_0^{1/2} \exp(iwV) U_0^{1/2}$ and characterized by a single parameter $\Lambda_{\mathrm{CBE}} = w^2 \langle |V_{kl}|^2 \rangle / D^2$ ($D = 2\pi/N$) and exact system symmetries [17,22]. The perturbation V belongs to a standard Gaussian ensemble of the Hermitian matrices, e.g., the Gaussian orthogonal ensemble (GOE), Gaussian unitary ensemble (GUE), etc. [17]. The circular Brownian ensemble analog of a QKR is given by the condition

$$\Lambda_{\mathrm{KR}} = \Lambda_{\mathrm{CBE}}. \tag{8}$$

As mentioned above, the studies [20,21] did not explore the infinite size limit of Λ_{KR} and its application for critical behavior analysis; we discuss this in the next section.

B. Critical behavior of quantum kicked rotor

For a critical point analysis of the QKR, we search for the system conditions leading to the critical eigenvalue statistics and the multifractal eigenfunctions in the infinite size limit ($N \to \infty$). The parametric conditions for the critical level statistics, characterized by a nonzero, finite Λ in the limit $N \to \infty$, can be obtained from Eqs. (6) and (7). The analysis suggests the possibility of several continuous families of critical points, characterized by the complexity parameter and the exact symmetries; we mention here only three main cases.

(i) $k \propto \sqrt{N}$, $\gamma = 0$, $\theta_0 = \pi/2N$. Equation (6) in this case leads to a size-independent $\Lambda_{\mathrm{KR,T}} = \chi^2/16$ with $\chi = k/\sqrt{N}$. For small k (in the mixed regime), this corresponds to a localization $\to$delocalization transition under time-reversal conditions (no parity symmetry) with a continuous family of critical points characterized by χ. The bulk statistics here is analogous to a circular Brownian ensemble U_w [see Eq. (8)] with $w = \chi\pi/2N$ [due to a GOE-type perturbation V with $|V_{kl}|^2 = (1+\delta_{kl})$ of a Poisson matrix [17]; see Eq. (8)]. The two ends of the transition in this case are the Poisson ($\Lambda \to 0$) and the COE ensembles ($\Lambda \to \infty$).

(ii) $\gamma_q \propto N^{-3/2}$, $\theta_0 = \pi/2N$. Equation (7) in this case gives $\Lambda_{\mathrm{KR,NT}} = \lambda^2/48\pi^2$ with $\lambda = \gamma_q N^{3/2}$. For large k (in the strongly chaotic limit), a finite λ gives the critical parameter for the transition from a time-reversible to a time-irreversible phase (both phases delocalized); it can be referred to as the weak-localization critical point. The end points of the transition are the COE ($\Lambda \to 0$) and the CUE ($\Lambda \to \infty$), with the critical statistics given by an intermediate circular Brownian ensemble with $w = \lambda/(2N\sqrt{3})$ (due to a GUE-type perturbation V, with $|V_{kl}|^2 = 1$, of a COE matrix [17]).

(iii) $\gamma = 0$, $\theta_0 \propto N^{-3/2}$. Here Eq. (6) gives $\Lambda_{\mathrm{KR,T}} = \phi^2 K^2/(64\pi^4 M^2)$ with $\phi = N^{3/2}\theta_0$ describing the critical point family for the transition from a parity-symmetric phase to a parity-fully-violated phase (both phases with time-reversal symmetry). For K in the mixed regime ($K < N\hbar$), a variation of ϕ leads to the Poisson $\to$ COE transition. For K in the strongly chaotic regime ($K > N\hbar$), the transition end points are the 2-COE [20] ($\Lambda \to 0$) and the COE ($\Lambda \to \infty$). The critical statistics for a specific K is given by the intermediate Brownian ensemble with $w = K\phi/(4\pi MN)$ (due to a GOE-type perturbation V, with $|V_{kl}|^2 = 1$, of the Poisson ensemble if $K \ll N\hbar$, or, the 2-COE ensemble if $K \gg N\hbar$).

As Eqs. (6) and (7) indicate, a size-independent Λ_{KR} can be obtained by other combinations of k, θ, γ too. This suggests critical behavior in the symmetry spaces other than those mentioned above.

The critical nature of the system for specific parametric conditions can further be confirmed by an analysis of the eigenfunction fluctuations. Studies of a wide range of systems (see [10–13] and the references therein) reveal the presence of strong fluctuations in the eigenfunctions near a critical point. The fluctuations can be characterized through a set of generalized fractal dimension D_q or $\tau_q = (q-1)D_q$, related to the scaling of the qth moment of the wave function intensity $|\phi(r)|^2$ with size N [11]: $P_q = \int dr |\phi(r)|^{2q} \propto N^{-\tau(q)/d}$. The multifractality of the eigenfunctions can also be analyzed through the spectrum of singularity strengths $f(\alpha)$ [10], related to $\tau(q)$ by a Legendre transformation: $f(\alpha(q)) = q\alpha(q) - \tau(q)$ (see [10,13] for details). In Sec. III, we numerically analyze both $\tau(q)$ and $f(\alpha)$ to detect the multifractality of the QKR eigenfunctions.

C. Anderson Hamiltonian and the complexity parameter

The Anderson model for a disordered system is described by a d-dimensional disordered lattice, of size L, with a Hamiltonian $H = \Sigma_n \epsilon_n a_n^\dagger a_n - \Sigma_{n \neq m} b_{mn} (a_n^\dagger a_m + a_n a_m^\dagger)$ in the tight-binding approximation [14]. In the site representation, H turns out to be a sparse matrix of size $N = L^d$ with the diagonal elements as the site energies $H_{kk} = \epsilon_k$ and the off-diagonals $H_{mn} = b_{mn}$ given by the hopping conditions. For a Gaussian-type on-site disorder (of variance ω and zero mean) and a nearest neighbor (NN) isotropic hopping with random (Gaussian) and/or nonrandom components, H can be modeled by an ensemble (later referred as the Anderson ensemble) with the following density:

$$\rho(H,v,b) = C\exp\left(-\sum_{k} H_{kk}^2/2\omega - \sum_{(k,l)=\mathrm{NN}} (H_{kl}-t)^2/2\eta\right) \times \prod_{(k,l)\neq \mathrm{NN}} \delta(H_{kl}) \tag{9}$$

with C as the normalization constant. As discussed in [19], the above ensemble can be rewritten as

$$\rho(H,h,b) = C\exp\left(-\sum_{k\leq l} (1/2h_{kl})(H_{kl}-b_{kl})^2\right), \tag{10}$$

where $b_{kk}=0$, $h_{kk}=\omega$, $b_{kl}=tf_{kl}$, $h_{kl}=\eta f_{kl}$ with $f(kl)=1$ for $\{k,l\}$ pairs connected by the hopping and $f(kl)\to 0$ for all $\{k,l\}$ pairs representing the disconnected sites. The single parameter Λ_{AE} governing the spectral statistics [see Eq. (19) of [19]] can then be given as

$$\Lambda_{\mathrm{AE}}(E,Y) = \left(\frac{|\alpha_w-\alpha_i|F^2}{\gamma_0}\right)\zeta^{2d}L^{-d} \approx \frac{|\alpha_w-\alpha_i|}{\gamma_0 N}\left(\frac{F}{I_2^{\mathrm{typ}}}\right)^2, \tag{11}$$

where

$$\alpha_w = \ln|1-\gamma_0\omega| + (z/2)\ln(|1-2\gamma_0\eta||t+\delta_{t0}|) \tag{12}$$

with z as the number of nearest neighbors, $\alpha_i=-\ln 2$, and γ_0 as an arbitrary constant. Further, $F(E)$ is the mean level density, ζ is the localization length, and I_2^{typ} is the typical inverse participation ratio: $I_2^{\mathrm{typ}}\propto\zeta^{-d}$.

III. NUMERICAL ANALYSIS

The objectives of our numerical analysis are twofold: (i) a search for the critical points of the quantum kicked rotor, and (ii) a comparison of its fluctuation measures with those of a three-dimensional Anderson ensemble. For this purpose, we analyze the following cases.

(i) *QKR1: quantum dynamics with time-reversal symmetry but parity symmetry broken* $k^2=\chi^2 N$, $\chi\approx 1.5$, $\gamma=0$, $\theta_0=\pi/2N$, $T=1$, $\tau=\hbar=40\pi/N$, which gives $K\approx 189/\sqrt{N}$. This case corresponds to the critical set (i) in Sec. II B. and is analyzed for many sizes ($N=213\to 1013$) to verify the critical behavior.

(ii) *QKR2: quantum dynamics with both time-reversal and parity symmetry broken*. $k\approx 20\,000$, $\gamma=\lambda_q N^{-3/2}$, $\lambda_q=6$, $T=1$, $\theta_0=\pi/2N$, $\tau=\hbar=40\pi/N$. This case belongs to set (ii) in Sec. II B and its critical nature is also confirmed by analyzing many N values.

(iii) *QKR3*. The same as QKR1 but with $\chi=0.8$ which gives $K\approx 100/\sqrt{N}$. We consider this case to verify the analogy with a $d=3$ Anderson ensemble.

(iv) *QKR4: quantum dynamics with time-reversal symmetry but parity symmetry broken*. $k\approx 4.5/\hbar$, $\gamma=0$, $\theta_0=\phi N^{-3/2}$, $\phi=0.84\pi^2$, $T=1$, $\tau=\hbar=8\pi/N$ [case (iii) in Sec. II B]. This is also analogous to the Anderson system mentioned above in the QKR3 case, notwithstanding the crucial changes in k and θ_0 for the two QKR cases.

To explore critical behavior, we analyze large ensembles of the matrices U for both QKR1 and QKR2 for various matrix sizes N; the ensemble in each case is obtained by varying k in a small neighborhood while keeping N fixed. The chosen N range gives K in the mixed regime for QKR1 ($6.25<K<13$) and in the chaotic regime for QKR2 ($1000<K<12\,000$). Prior to the analysis, the quasienergies (the eigenvalues of U) are unfolded by the local mean level density D^{-1} ($=N/2\pi$, a constant due to repulsion and the unit-circle confinement of the quasienergies). Figures 1 and 2 display the nearest-neighbor spacing distribution $P(s)$ and the number variance $\Sigma^2(r)$, the measures of the short- and long-range spectral correlations, respectively, for QKR1 and QKR2. Note that the curves in Fig. 1 are intermediate between the Poisson and the COE limits; the size independence implies their survival in the infinite size limit too. This indicates QKR1 as the critical point of transition from a localized to a delocalized phase. Similarly the curves in Fig. 2, intermediate between the COE and the CUE limits, suggest QKR2 as the critical point of transition from the time-reversed phase to the time-irreversible phase (both phases in the chaotic regime).

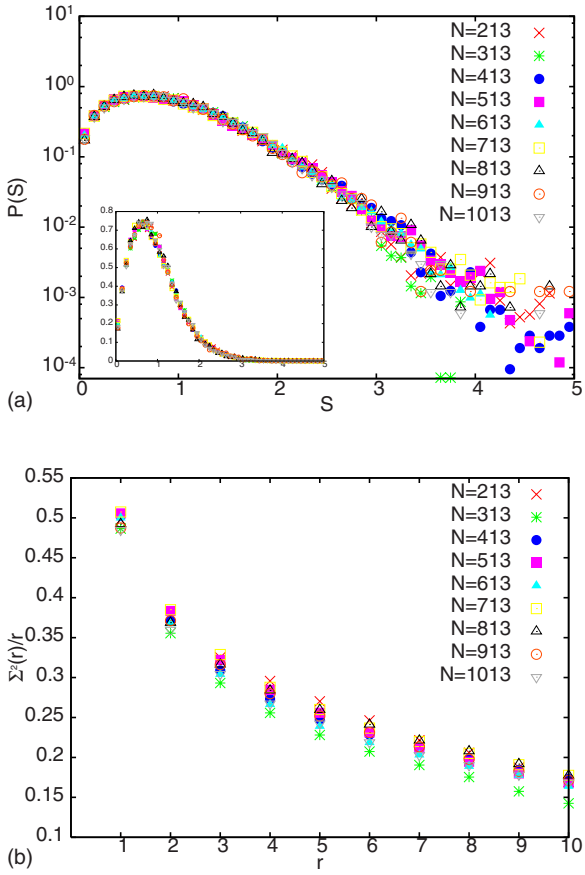

FIG. 1. (Color online) Spectral measures of QKR1. (a) nearest-neighbor spacing distribution $P(S)$ of the eigenvalues for various sizes N, with inset showing behavior on the linear scale; (b) number variance $\Sigma^2(r)$ for various sizes. The convergence of the curves for different sizes indicates scale invariance of the statistics. The behavior is critical, being different from that of the two end points, namely, Poisson and CUE statistics, even in the infinite-size limit.

To reconfirm the critical nature of QKR1 and QKR2, we numerical analyze the moments of their local eigenfunction intensity for various sizes. The results shown for τ_q in Figs. 3(a) and 4(a) indicate the multifractal nature of the

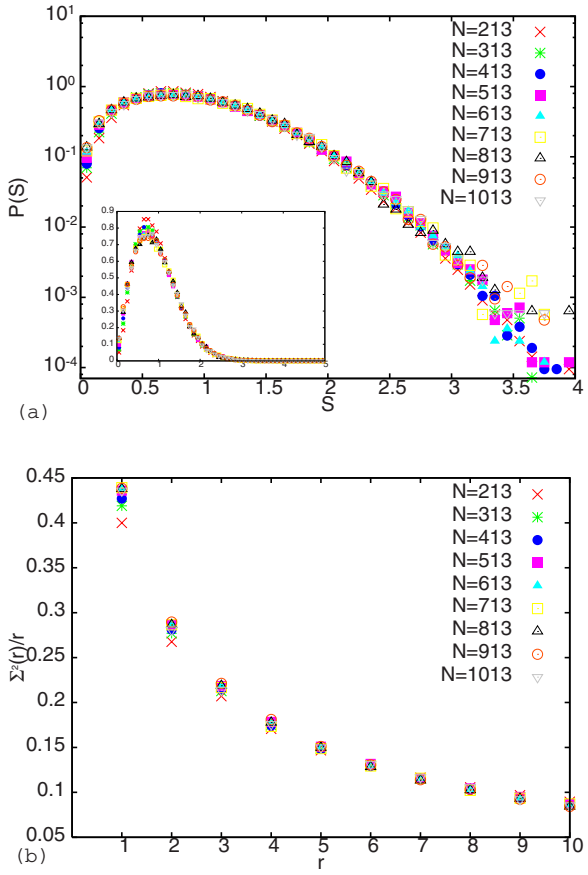

FIG. 2. (Color online) Spectral measures of QKR2. (a) Distribution $P(S)$ of the nearest-neighbor eigenvalue spacings S for various sizes, with inset showing behavior on the linear scale; (b) number variance $\Sigma^2(r)$ for various sizes. Again, the statistics being intermediate between COE and CUE and convergence of the curves for different sizes indicate its critical behavior.

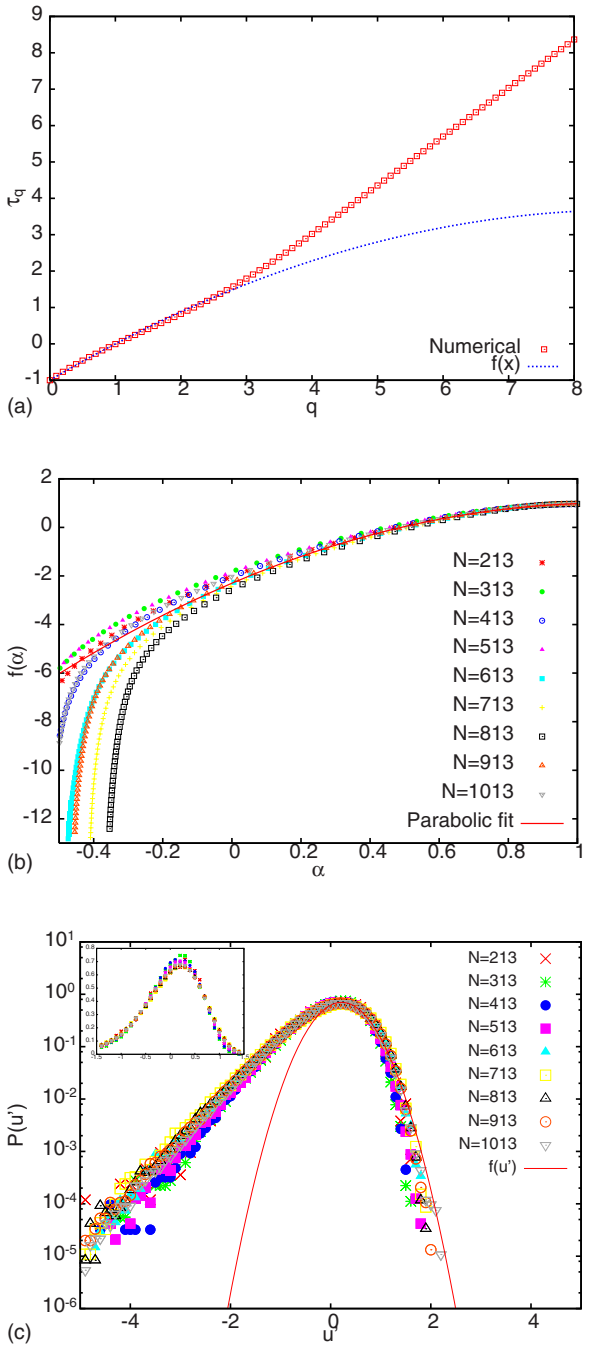

FIG. 3. (Color online) Multifractality of QKR1. (a) Fractal dimension τ_q along with the fit $y(q)=(1+c)q-1-cq^2$ with $c=0.06$ (good only for $q\leqslant 3$). A fit for the large-q regime suggests the behavior $\tau_q=q-1+0.02q^2$. (b) Multifractal spectrum $f(\alpha)$ for various sizes along with the parabolic fit $f(\alpha)=d-(\alpha-\alpha_0)^2/4(\alpha_0-d)$ with $\alpha_0=1.09$ and $d=1$. (c) Distribution $P_u(u')$ with $u'=(\ln u-\langle\ln u\rangle)/\langle\ln^2 u\rangle$ of the local intensity of an eigenfunction for QKR1. The solid line represents the function $f(u')$ given by Eq. (13) with $a=5.2$, $b=1.2$, and $c=0.78$ [corresponding to an approximate log-normal behavior of $P_u(u)$], a good approximation in the tail region as expected. The inset shows the behavior on a linear scale.

eigenfunctions; for small-q ranges, τ_q shows the behavior $\tau_q=(1+c)q-d-cq^2$ (or $D_q=1-cq$) with $d=1$ and $c=0.06,0.075$ for QKR1 and QKR2, respectively (see Table I for the first few values of D_q). These results are reconfirmed by a numerical study of the $f(\alpha)$ spectrum displayed in Figs. 3(b) and 4(b). For this purpose, we use the procedure based on the evaluation of moments, described in [13] [using Eqs. (4) and (10) of [13]] which has the advantage of full control over the finite-size corrections. The numerical results for α_0, α_1, and $\alpha_{1/2}$ for the QKR (see Table I) indicate a parabolic form of $f(\alpha)$ [also confirmed by the fits shown in Figs. 3(b) and 4(b)] and therefore a log-normal behavior of the local eigenfunction intensity $u=|\psi(r)|^2$ for large-u regions (see [10,11,13] for details). As shown in Figs. 3(c) and 4(c), the tail behavior of $P_u(u')$ can be well approximated by the function

$$f(u') = \sqrt{a/2\pi}e^{b+au'}e^{-a(u'+c)^2/2} \tag{13}$$

with $u'=(\ln u-\langle\ln u\rangle)/\langle\ln^2 u\rangle$ [see Figs. 3(c) and 4(c) for numerical values of a,b,c].

The bulk statistical behavior of the Hermitian matrices is known to be analogous to the unitary matrices [17,22]. This, along with the single parametric formulation of the statistics of the Hermitian matrix ensemble [15], suggests the analogy of the QKR and Anderson ensemble statistics if their Λ pa-

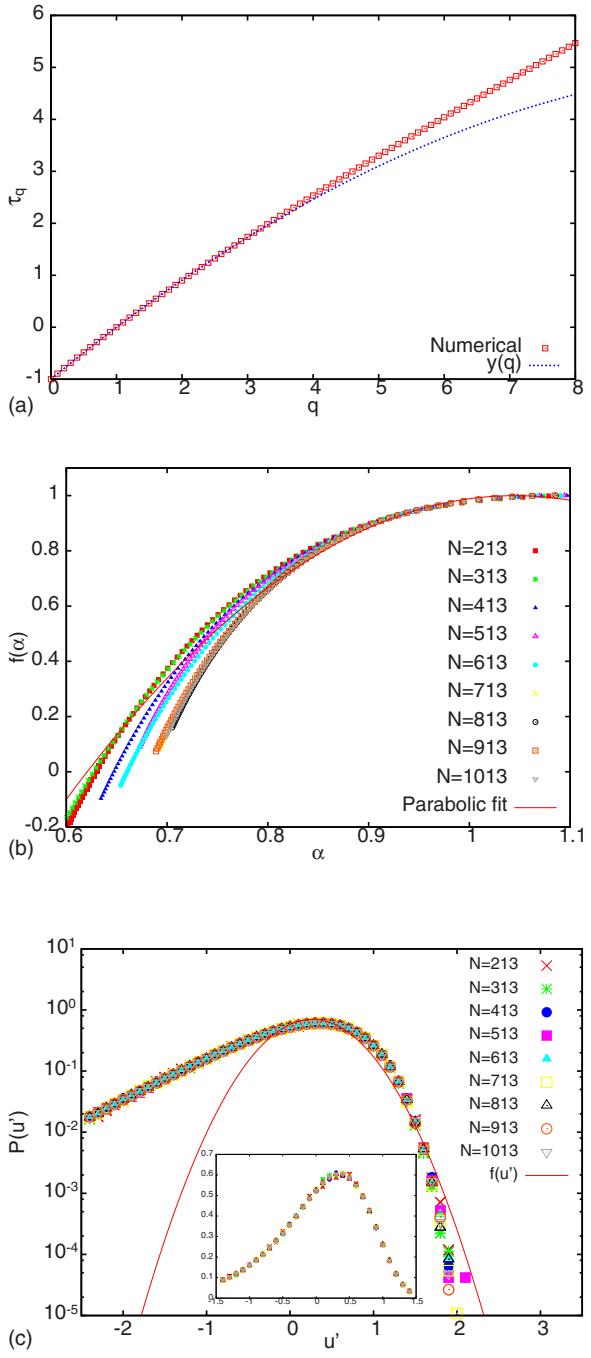

FIG. 4. (Color online) Multifractality of QKR2. (a) Fractal dimension τ_q along with the fit $y(q)=(1+c)q-1-cq^2$ with $c=0.075$ (good only for $q<4$). (b) Mulifractal spectrum $f(\alpha)$ for various sizes along with a parabolic fit, of the same form as in Fig. 3(b) with $\alpha_0=1.045$ and $d=1$. (c) Distribution $P_u(u')$ of the local intensity of an eigenfunction for QKR2, with u' the same as in Fig. 3(c). The solid line represents the function $f(u')$ with $a=5.3$, $b=0.95$, and $c=0.73$ [corresponding to a log-normal behavior of $P_u(u)$], which fits well in the tail region of $P_u(u')$. The inset shows the behavior on a linear scale.

rameters are equal (in addition to similar global constraints, e.g., global symmetries) [16]. Our next step is a comparison of the fluctuation measures of a time-reversal Anderson case with QKR3, a time-reversal system with a partially localized

TABLE I. Multifractality analysis of the QKR: α values here are obtained by an $L\to\infty$ extrapolation of α_L [13]. The $0<D_2<1$ behavior indicates the multifractal nature of the three QKR cases.

	Case		
	QKR1	QKR2	QKR3
α_0	1.034	1.008	2.466
$\alpha_{1/2}$	1.007	1.001	0.812
α_1	0.934	0.991	0.543
D_0	1	1	1
D_1	0	0	0
D_2	0.825	0.811	0.89

wave dynamics in the momentum space (dynamical localization). For this purpose, we analyze a cubic ($d=3$) Anderson lattice of linear size L ($N=L^d$) with a Gaussian site disorder (of variance $\omega=W^2/12$, $W=4.05$, and mean zero), the same for each site, an isotropic Gaussian hopping (of variance $\eta=1/12$ and mean zero) between nearest neighbors with hard wall boundary conditions; these conditions correspond to the critical point for a disorder-driven metal-insulator transition [19]. A substitution of the above values (with $t=0$) in Eq. (12) gives $\alpha_w-\alpha_i=1.36$. As shown by the numerical analysis in [19,25], $F(E)\approx 0.26e^{-E^2/5}$ and $I_2^{\rm typ}\approx 0.04$, which on substitution in Eq. (11) gives $\Lambda_{\rm AE}=0.056$ (with $\gamma_0=2$).

For the AE-QKR comparison, we analyze the ensembles of 2000 matrices with matrix size $N=L^3=512$ for the three-dimensional AE case and $N=513$ for the QKR case. The energy dependence of Λ (see [19,20]) forces us to confine our analysis to only 10% of the levels near the band center from each such matrix. The levels are unfolded by respective local mean-level density in each case (so as to compare the level density fluctuations on a same density scale) [17]. Figure 5(a) shows the AE-QKR3-QKR4 comparison of $P(s)$; the good agreement among the three curves verifies the Λ dependence of the spectral correlations. This is reconfirmed by Fig. 5(b), showing a comparison of the number variance. Note that $\phi\approx 0.84\pi^2$ for QKR4 is the same as the theoretical analog given by the condition $\Lambda_{\rm KR,T}=\Lambda_{\rm AE}=0.056$ [see Eqs. (6) and (11)]. However, $\chi=0.8$ for QKR3 shows a small deviation from the theoretical prediction ($\chi\approx 0.95$). This may be because Eq. (6) is a poor approximation at the integrable-nonintegrable boundary $K=0$. Note that the classical limits of QKR3 and QKR4 are different ($K=0$ for QKR3, $K=4.5$ for QKR4), although their semiclassical K are the same ($K=4.5$ with $N=513$ for QKR3, $K=4.5$ for any N for QKR4). As is clear from Eq. (2), $K=0$ marks the boundary between the integrable and mixed dynamics; $K=4.5$ corresponds to the mixed nature of the dynamics [see Fig. 5(c)].

As discussed in [25], the eigenfunction fluctuations of finite systems are influenced by two parameters, namely, system size N as well as $\Lambda_{\rm measure}$. To compare the $\Lambda_{\rm measure}$ dependence of an eigenfunction measure, therefore, the same system size should be taken for each system. Figure 6(a) shows the distribution $P_u(u')$ of the local eigenfunction intensity $u'=(\ln u-\langle\ln u\rangle)/\langle\ln^2 u\rangle$ for the AE and QKR3. The close proximity of the two curves suggests $\Lambda_{\rm KR,T}$ as the pa-

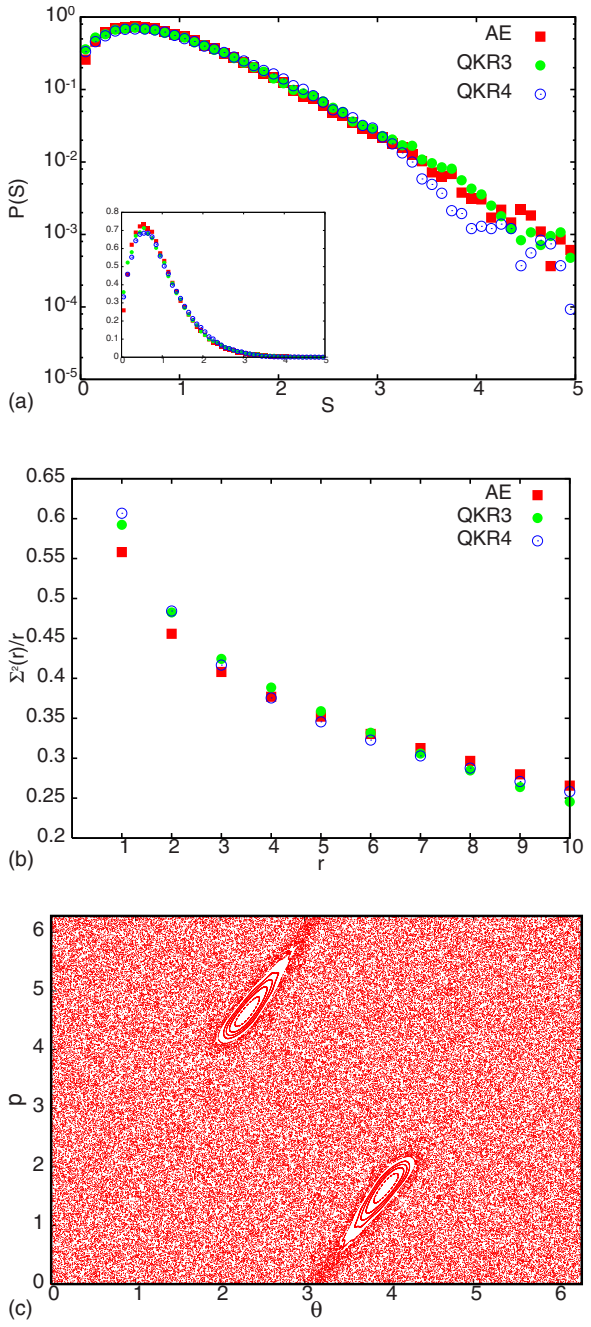

FIG. 5. (Color online) Comparison of spectral statistics of the Anderson ensemble with QKR3 and QKR4. (a) $P(S)$, with inset showing the linear behavior; (b) $\Sigma^2(r)$. Note that the statistics for QKR3 and QKR4 turn out to be close to that suggested by the relation $\Lambda_{AE}=\Lambda_{KR,T}$ (giving $\chi=0.95$ for QKR3 and $\phi=0.84\pi^2$ for QKR4). (c) Phase-space behavior of the classical kicked rotor at $K=4.5$ [see Eq. (2)].

rameter governing the local eigenfunction intensity too (we have verified the analogy also with QKR4). A comparison of the AE-QKR3 multifractality spectrum, shown in Fig. 6(b), reconfirms their close similarity at least on statistical grounds.

The numerical confirmation of the statistical analogy of QKR4-AE-QKR3 systems supports our claim regarding single parametric (Λ) dependence of the statistics apart from

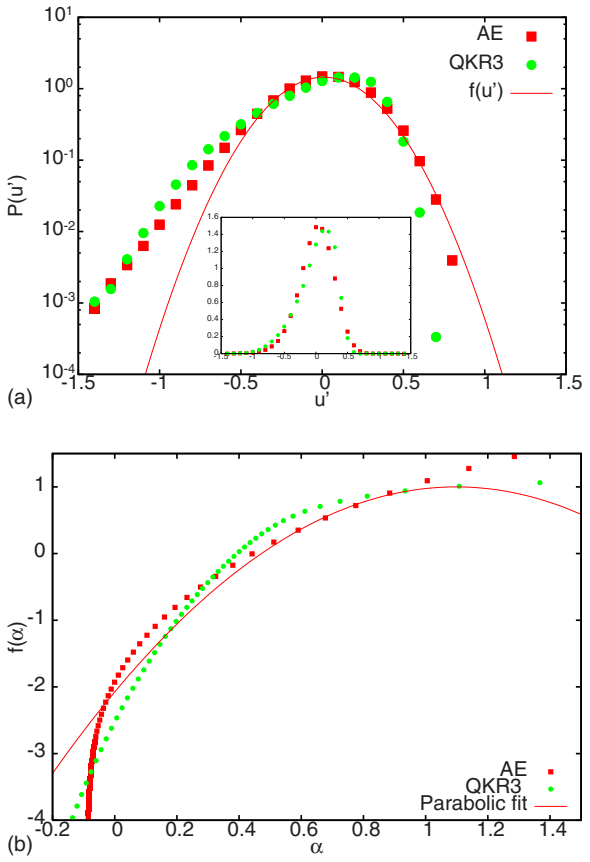

FIG. 6. (Color online) Comparison of the multifractality of the eigenfunctions of QKR3 with the Anderson ensemble. (a) Local intensity distribution $P_u(u')$ of an eigenfunction with u' the same as in Figs. 3 and 4. Also shown is the function $f(u')$ with $a=15.9$, $b=7.7$, $c=0.99$, a good fit in the tail region of $P_u(u')$. The inset shows the behavior on a linear scale. (b) Multifractal spectrum $f(\alpha)$; note that the QKR3 analog of the Anderson ensemble here is the same as the one in Fig. 5. Again the fit has the same parabolic form as in Figs. 3 and 4, with $\alpha_0=1.1$ and $d=1$.

global constraints. Note that the latter are the same for both QKR3 and QKR4 (i.e., parity symmetry violated, time-reversal symmetry preserved, and mixed dynamics) which results in their statistics being intermediate to the same universality classes, namely, Poisson and COE, although the transition parameters are different in the two cases.

The QKR-AE analogy can be utilized to connect them to other complex systems too. In [19,25], we studied the AE connection with the PRBME [described by $\langle H_{kl}\rangle=0$, $\langle H_{kl}^2\rangle \propto (1+|k-l|^2/p^2)^{-1}$ [18]] and the GBE ($\langle H_{kl}\rangle=0$, $\langle H_{kl}^2\rangle \propto (1+cN^2)^{-1}$ [19]). For the AE case considered above, the PRBME and the GBE analogs for the spectral statistics turned out to be $p=0.4$ and $c=0.1$; these systems are therefore the spectral statistical analogs of QKR3 and QKR4 as well as of an $N\times N$ circular Brownian ensemble with $w\approx 0.4\pi N^{-1}$ [see case(i) of Sec. II B].

IV. CONCLUSION

To summarize, we studied the statistical analogy of two paradigmatic models of dynamical and disordered systems,

namely, the quantum kicked rotor and the Anderson Hamiltonian, in partially localized regimes. Our results indicate the existence of critical behavior in the classically mixed regime of the QKR with a smooth potential. This is qualitatively analogous to a disorder-driven metal-insulator transition in the Anderson system; the quantitative analogy for their statistical behavior follows if their complexity parameters are equal. Our study also reveals the possibility of other transitions in the QKR, e.g., from a symmetry-preserving phase to a symmetry-fully-violated phase. These transitions are analogous to similar symmetry-breaking transitions in disordered metals, e.g., the Anderson Hamiltonian in the weak disorder limit in the presence of a slowly varying magnetic field.

As with the Anderson transition, the QKR transitions are governed by the complexity parameter Λ too. However, in contrast to the Λ derivation for the Anderson case by an ensemble route, Λ for the QKR is derived by a semiclassical method. The semiclassical Λ formulation is also numerically verified for the QKR ensembles. This indicates the equivalence of the ensemble averaging and the phase-space averaging for the statistical analysis. This further lends credence to the single parametric formulation of the statistical behavior of complex systems, irrespective of the origin of their complexity. However, it needs to be examined for other dynamical systems.

Research has indicated a multiparametric dependence of the spectral statistics at long energy scales of dynamical systems [26], originating in level-density oscillations due to the short periodic orbits. However, these studies are not at variance with our work. This is because the semiclassical Λ derivation in [20] is based on the assumed equivalence of the traces of the operators with their phase-space averages. The assumption may not be valid on short time scales of the dynamics. One should also understand the exact role of the ensemble averaging for the statistical analysis of dynamical systems.

ACKNOWLEDGMENT

We would like to express our gratitude to Professor M. V. Berry for many helpful suggestions.

[1] B. V. Chirikov, Phys. Rep. **52**, 263 (1979); G. Casati and L. Molinary, Prog. Theor. Phys. Suppl. **98**, 287 (1989); U. Gerland, Phys. Rev. Lett. **83**, 1139 (1999).
[2] F. Izrailev, Phys. Rep. **196**, 299 (1990).
[3] Y. V. Fyodorov and A. D. Mirlin, Int. J. Mod. Phys. B **8**, 3795 (1994).
[4] M. Thaha and R. Blumel, Phys. Rev. Lett. **72**, 72 (1994).
[5] I. Pizorn, T. Prosen, S. Mossmann, and T. H. Seligman, New J. Phys. **10**, 023020 (2008).
[6] S. Fishman, D. R. Grempel, and R. E. Prange, Phys. Rev. Lett. **49**, 509 (1982).
[7] B. V. Chirikov, F. M. Izrailev, and D. L. Shepelyansky, Physica D **33**, 77 (1988).
[8] G. Casati, B. V. Chirikov, I. Guarneri, and F. M. Izrailev, Phys. Rev. E **48**, R1613 (1993); G. Casati, L. Molinari, and F. M. Izrailev, Phys. Rev. Lett. **64**, 1851 (1990); K. Zyczkowski, M. Lewenstein, M. Kus, and F. Izrailev, Phys. Rev. A **45**, 811 (1992). C. E. Creffield, G. Hur, T. S. Monteiro, Phys. Rev. Lett. **96**, 024103 (2006).
[9] A. M. Garcia-Garcia and J. Wang, Phys. Rev. Lett. **94**, 244102 (2005); **100**, 070603 (2005); Acta Phys. Pol. A **112**, 635 (2007).
[10] M. Janssen, Phys. Rep. **295**, 1 (1998).
[11] C. Castellani and L. Peliti, J. Phys. A **19**, L429 (1986); F. Wegner, Nucl. Phys. B **280**, 210 (1987).
[12] E. Cuevas, Phys. Rev. B **68**, 184206 (2003); **68**, 024206 (2003).
[13] F. Evers, A. Mildenberger, and A. D. Mirlin, Phys. Rev. B **64**, 241303(R) (2001).
[14] P. Lee and T. V. Ramakrishnan, Rev. Mod. Phys. **57**, 287 (1985).
[15] P. Shukla, Phys. Rev. E **71**, 026226 (2005); **75**, 051113 (2007); **62**, 2098 (2000).
[16] P. Shukla, J. Phys. A **41**, 304023 (2008).
[17] M. L. Mehta, *Random Matrices* (Academic Press, New York, 1991); C. E. Porter, *Statistical Theory of Spectra: Fluctuations* (Academic Press, New York, 1965); F. Haake, *Quantum Signatures of Chaos* (Springer, Berlin, 1991).
[18] A. D. Mirlin, Y. V. Fyodorov, F.-M. Dittes, J. Quezada, and T. H. Seligman, Phys. Rev. E **54**, 3221 (1996).
[19] P. Shukla, J. Phys.: Condens. Matter **17**, 1653 (2005).
[20] P. Shukla and A. Pandey, Nonlinearity **10**, 979 (1997); A. Pandey, R. Ramaswamy, and P. Shukla, Pramana, J. Phys. **41**, L75 (1993).
[21] P. Shukla, Phys. Rev. E **53**, 1362 (1996).
[22] A. Pandey and P. Shukla, J. Phys. A **24**, 3907 (1991).
[23] J. Tworzydlo, A. Tajic, and C. W. J. Beenakker, Phys. Rev. B **70**, 205324 (2004); **69**, 165318 (2004).
[24] F. M. Izrailev, Phys. Rev. Lett. **56**, 541 (1986).
[25] P. Shukla, Phys. Rev. E **75**, 051113 (2007).
[26] M. V. Berry, Proc. R. Soc. London, Ser. A **400**, 229 (1985).